33rd Annual International Conference of the IEEE EMBS
Boston, Massachusetts USA, August 30 - September 3, 2011

High Temporal Resolution Dynamic Contrast-Enhanced MRI at 7 Tesla: A Feasibility Study with Mouse Liver Model

S. Hartono, C. H. Thng, Q. S. Ng, C. X. Yong, C.-T. Yang, W. Shi, K. H. Chuang, and T. S. Koh

Abstract— **Dynamic contrast-enhanced magnetic resonance imaging (DCE-MRI) has been widely applied to evaluate microcirculatory parameters in clinical settings. However, pre-clinical studies involving DCE-MRI of small animals remain challenging with the requirement for high spatial and temporal resolution for quantitative tracer kinetic analysis. This study illustrates the feasibility of applying a high temporal resolution (2 s) protocol for liver imaging in mice by analyzing the DCE-MRI datasets of mice liver with a dual-input two-compartment tracer kinetic model. Phantom studies were performed to validate the T_1 estimates derived by the proposed protocol before applying it in mice studies. The DCE-MRI datasets of mice liver were amendable to tracer kinetic analysis using a dual-input two-compartment model. Estimated micro-circulatory parameters were consistent with liver physiology, indicating viability of applying the technique for pre-clinical drug developments.**

I. Introduction

DYNAMIC contrast-enhanced (DCE) imaging involves intravenous injection of a contrast tracer and sequential imaging to monitor the flow of tracer in the tissue of interest and a feeding artery. With advances in fast imaging techniques and developments in tracer kinetic modeling, *in vivo* assessment of organ microcirculation using DCE imaging by computed tomography (DCE-CT) or magnetic resonance imaging (DCE-MRI) has become more realistic in the clinical settings [1, 2].

Recently, DCE-MRI with tracer kinetic modeling has been proposed as a biomarker for assessment of tumor angiogenesis in clinical trials [3-5]. There is a need to perform similar experiments in mice to explore anti-angiogenic drug mechanism and evaluate drug efficacy. However, DCE-MRI in a small animal is challenging due to several difficulties, such as a small field of view with high spatial resolution, limited venous access, low injection rate, high heart rate and fast circulation time. On the other hand, it is also recognized that a DCE MRI protocol with high temporal resolution is needed for animal studies, as a sub-second temporal resolution is needed to characterize the first pass of tracer satisfactorily [6]. However, previous DCE-MRI studies in high-field animal scanners were typically performed with lower temporal resolutions of about 3.6 sec to more than one minute [7-9].

In this work, we explore the feasibility of applying a high spatial and temporal resolution (2 s) DCE-MRI protocol for arterial concentration estimation and perfusion imaging in mice. Phantom studies were performed to validate T_1 and contrast agent concentration estimates derived by the proposed protocol. The study was done in normal mice liver, as similar studies have been done in human liver and hence it would facilitate a more convenient translation from human study to animal study [10]. The mice liver DCE-MRI datasets were analyzed using dual-input version of standard two-compartmental model [11].

II. Materials and Methods

A. Mice

Five male C57BL/6 mice (6 weeks old, 30 ± 2 g) were used in this study. Mouse core body temperature was monitored with a rectal probe and maintained at 37 ± 0.3 °C by a feedback-controlled warm-air heating system. The mice were kept under 1-2 % isoflurane anesthesia during MR scanning.

This study was approved by the local Institutional Animal Care and Use Committee. All mice were maintained according to the guidelines for the Care and Use of Laboratory Animals published by the National Institutes of Health.

B. DCE-MRI

MR images were acquired on a 7T animal MR scanner (Bruker ClinScan, Bruker BioSpin MRI GmbH, Ettlingen, Germany). A three-dimensional (3D) dataset was obtained using a T_1-weighted gradient echo sequence (FLASH 3D VIBE) with repetition time TR = 3.04 ms, echo time TE = 1.23 ms, field of view FOV = 36 × 36 mm, acquisition matrix of 128 × 128, eight slices (voxel size of 0.28 × 0.28 × 1 mm), and temporal resolution of 2 s per acquisition.

The dynamic imaging protocol consists of 10 baseline acquisitions with two flip angles of 6° and 14° (five times each), followed by the manual injection of 50 μL of Gd-DOTA (Dotarem, Guerbet S.A., Villepinte, France) through the tail vein. Post-contrast 3D T_1-weighted scans of flip angle 14° were performed 130 times over a 4 minutes and 20 seconds period. The contrast was injected at the first post-contrast acquisition.

Manuscript received March 24, 2011. This work was supported in part by the Biomedical Research Council of Singapore under Grant 08/1/31/19/577.

S. Hartono is with the National Cancer Centre Singapore and Nanyang Technological University, Singapore (phone: 65-82269485; e-mail: sept0004@e.ntu.edu.sg).

C. H. Thng and Q. S. Ng are with the National Cancer Centre Singapore (e-mail: dditch@nccs.com.sg and ng.q.s@nccs.com.sg).

C. X. Yong, C.-T. Yang, and K. H. Chuang are with the Singapore Bioimaging Consortium (e-mail: yong_cai_xian@sbic.a-star.edu.sg, yang-changtong@sbic.a-star.edu.sg, and chuang_kai_hsiang@sbic.a-star.edu.sg).

W. Shi is with the Nanyang Technological University, Singapore and Jinan University, China (e-mail: wshi1989@gmail.com).

T. S. Koh is with the National Cancer Centre Singapore and Nanyang Technological University, Singapore (e-mail: etskoh@ntu.edu.sg).

978-1-4244-4122-8/11/$26.00 ©2011 IEEE

C. Phantom Validation

At low concentrations, contrast agent concentration C can be estimated by the difference in longitudinal relaxation rates,

$$r_1 C = \frac{1}{T_1^C} - \frac{1}{T_1^0} \quad (1)$$

where T_1^C and T_1^0 are the post-contrast and pre-contrast (native) T_1 values, respectively, and r_1 denotes the longitudinal relaxivity. A phantom study was performed to validate the T_1 values estimated by the above dual flip angle protocol by comparing with those derived from inversion recovery measurements (inversion time TI = 50, 100, 200, 400, 600, 800, 1000, 1500, 2000, 4000 ms; repetition time TR = 5000 ms). The phantom consists of tubes of saline diluted with 0.05 g/L of copper sulphate to mimic T_1 value in human body tissue at 1.5 sec and filled with various concentration of Dotarem at 0.01, 0.05, and 0.1 mM.

D. Tracer Kinetic Modeling

Consider a bi-compartmental tissue system where the first compartment represents the vascular space and the second compartment represents the interstitial space. Assuming well-mixed compartments, tracer concentration in each compartment at time t is given as follows [11]:

$$v_1 \frac{d}{dt} C_1(t) = F\rho\big(C_{in}(t) - C_1(t)\big) - PS\rho(C_1(t) - C_2(t)) \quad (1)$$

$$v_2 \frac{d}{dt} C_2(t) = PS\rho(C_1(t) - C_2(t)) \quad (2)$$

where F denotes blood flow, C_1 and C_2 denote tracer concentration in the vascular and interstitial space, respectively, PS denotes the permeability surface-area product, and denotes the tissue of density, which is set at 1 g/ml. v_1 is the fractional vascular volume, v_2 is the fractional interstitial volume, and $C_{in}(t)$ denotes the arterial input concentration.

The operational equation for analysis of the DCE imaging data can be expressed as

$$C_{tiss}(t) = FC_{in}(t) \otimes R(t) \quad (3)$$

where Ctiss denotes the tracer concentration in the tissue voxel and ⊗ denotes the convolution operator. $R(t)$ is the impulse residue response function, which describes the fractional amount of tracer remaining in the tissue owing due to an impulse input at time t. And $R(t)$ is given by

$$R(t) = A\exp(s_1 t) + (1 - A)\exp(s_2 t) \quad (4)$$

where s_1 and s_2 are the solutions of the following quadratic equation:

$$s^2 + \left(\frac{PS\rho}{v_1} + \frac{PS\rho}{v_2} + \frac{F\rho}{v_1}\right)s + \frac{PS\rho}{v_2}\frac{F\rho}{v_1} = 0 \quad (5)$$

and

$$A = \frac{s_1 + \frac{PS\rho}{v_1} + \frac{PS\rho}{v_2}}{s_1 - s_2} \quad (6)$$

E. Dual Input Model

Consider two sources of blood flow to the liver: flow from the hepatic artery F_A and flow from the portal vein F_{PV}. Assuming that the tracer concentration-time curves for the hepatic artery $C_A(t)$ and the portal vein $C_{PV}(t)$ can be sampled from dynamic MR images, the total input concentration-time curve $C_{in}(t)$ can be expressed as follows [10]:

$$C_{in}(t) = aC_A(t) + (1 - a)C_{PV}(t) \quad (9)$$

where a (= F_A/F) denotes the arterial fraction. The total hepatic blood flow, F, then is given as the sum of F_A and F_{PV}.

F. Data Processing

Post-processing was performed off-line on an Intel® Core™2 Duo personal computer with Matlab™ (MathWorks, Natick, MA). For each case, region of interest corresponding to the liver within the central six (of eight) imaging slices were manually outlined by an experienced radiologist.

The hepatic arterial input $C_A(t)$ was approximated by sampling the concentration-time curve at the aorta and the portal venous input $C_{PV}(t)$ was sampled from the portal vein. $C_A(t)$ and $C_{PV}(t)$ were divided by a factor of (1 – Hct), where Hct is the fractional hematocrit for mice and was set at 45% [12, 13]. To generate the parameter maps, the tissue concentration-time curve $C_{tiss}(t)$ for each voxel within the outlined region of interest was fitted using Equation 3 for the standard two-compartmental model.

III. Results and Discussion

The parameters of DCE-MRI sequences used in human studies and its translated version in animal studies were given in Table I. The sequences were based on a similar basic FLASH sequence. The values of TR and TE were set to be as similar as possible within the allowances given by the machine.

The comparison between T_1 values derived by the inversion recovery sequence with those estimated by the dual flip angle method was given in Figure 1. A linear correlation with slope of 1.22 and negligible ordinate intercept was obtained. Hence a reasonable precision of T_1 values estimated by the latter method was acquired and indicated the reliability of the estimated concentration values in the mouse tissue.

TABLE I
DCE-MRI Parameters in Human and Animal

Parameters	Human	Animal
Machine	Avanto (1.5T, Siemens)	ClinScan (7T, Bruker)
Platform	syngoMR	syngoMR
Sequence	FLASH 3D	FLASH 3D VIBE
FoV	40 x 40 cm	36 x 36 mm
TR	3.03 ms	3.04 ms
TE	1.17 ms	1.23 ms
Temp. resolution	1.38 s	2 s
Slice	6	8
Slice thickness	8 mm	1 mm
Base resolution	256 x 256	128 x 128
Flip angle	6° & 18°	6° & 14°

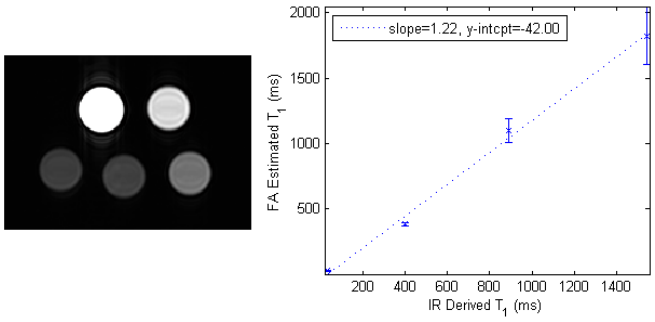

Fig. 1. (a) Phantom setup, positioned as followed from the bottom left corner, moving counter-clockwise: saline, saline with 0.05 g/L of copper sulphate (solution 'A'), 'A' added with 0.01, 0.05, and 0.01 mmol/mL of Dotarem, respectively, and (b) comparison between T_1 derived by the inversion recovery sequence with T_1 estimated by multiple flip angle method

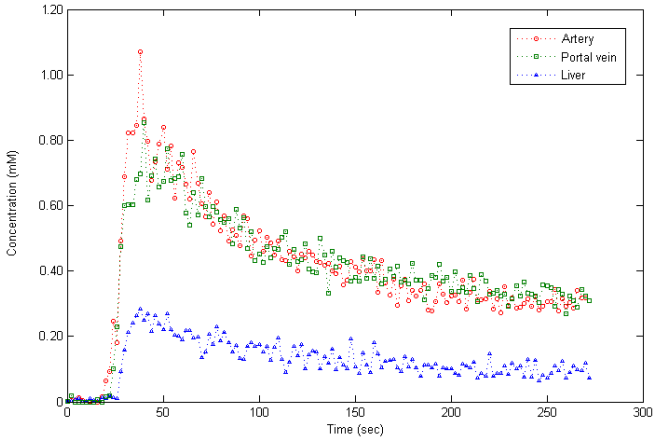

Fig. 2. Signal concentration time-curves in the artery, portal vein, and liver tissue of Mouse 01

A typical set of signal-time concentration profiles in the artery, the portal vein, and the liver tissue was given in Fig. 2. The profiles were similar with the findings previously reported in human studies [10]. The order of arrival of the contrast was as follow: in the artery, in the portal vein, and in the liver tissue. It showed that the two vascular inputs mix in the sinusoids at different time intervals. However, current temporal resolution of image acquisition of two seconds might not be adequate in delineating the difference clearly.

The microcirculatory parameters derived from the standard two-compartmental model were presented in Table II. The extravasation parameters derived from the model such as v_2 and PS were zero or close to zero for all cases. They corresponded with the results previously observed in human studies [10] and agreed with the murine physiology [14-17]. The liver is a highly vascular organ that consists of a series of fenestrated sinusoids which function as the vascular space. The sinusoids are predominantly supplied by the portal vein (80%) and supplemented by the hepatic artery (20%) [18, 19]. They are separated from the liver cords by the Space of Disse, which are comprised of two rows of closely apposed hepatocytes. The Space of Disse may then be considered as an interstitial space within the liver. However, due to the large size of the fenestrae of the sinusoids, low-molecular weight compounds such as gadolinium contrast can trace freely between the vascular space (sinusoids) and the interstitial space (Space of Disse). Both of them then effectively function as a single compartment system [2, 20]. Hence low values of fractional interstitial volume and permeability-surface area product in normal liver were expected, as were observed in this study.

The parametric maps of Mouse 03 were given in Figure 3 and a relatively monotonic distribution of v_2 and PS could be observed in Fig. 3 (b) and (d), thus confirming the single compartment system of normal liver.

The mono-compartmental system can be inferred as well from the signal concentration-time curve profile in the liver tissue in Fig. 4, as a contrast uptake enhancement pattern of a rapid increase which was followed by rapid washout was observed [21]. Figure 4 also showed an example of fitting the dual-input conventional compartmental model to liver tissue concentration-time curve and the impulse residual function R(t) corresponding to the fitting of the enhancement pattern.

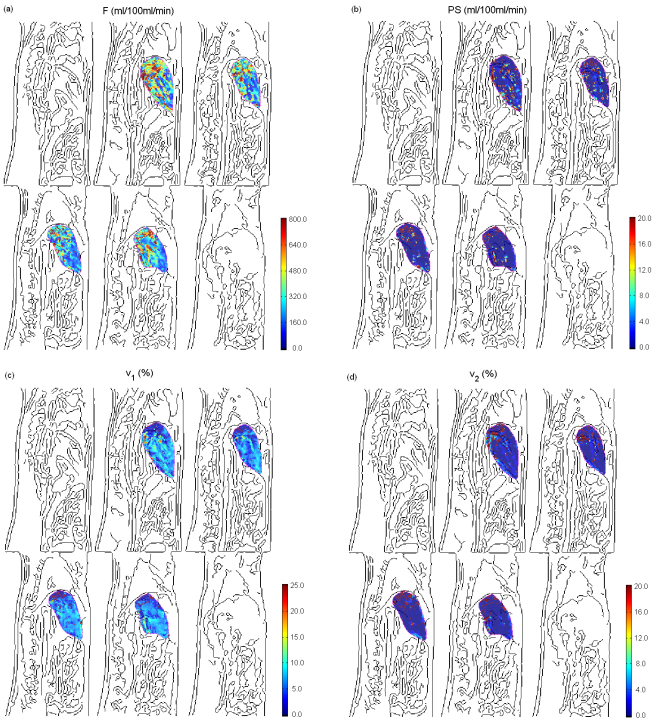

Fig. 3. Parametric maps of (a) blood flow, (b) permeability-surface area product, (c) fractional intravascular space, and (d) fractional extravascular extracellular space for Mouse 03 (slice 2 to 7)

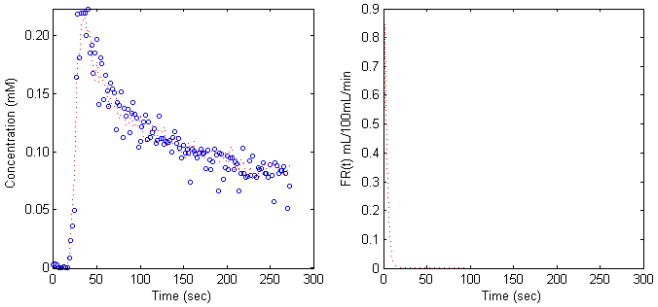

Figure 4. (a) Example of fitting the dual-input conventional compartmental model to liver tissue concentration-time curve and (b) impulse residual function R(t) corresponding to the fitting of the enhancement pattern. F = 220.6 mL/100mL/min, t_1 = 2.58 sec, = 25.7%, v_1 = 9.5%, v_2 = 0%, PS = 0.

TABLE II
MEDIAN VALUES OF MICROCIRCULATORY PARAMETERS AS DERIVED BY THE STANDARD TWO-COMPARTMENT MODEL

2-compartment model		M01	M02	M03	M04	M05
F	(ml/100ml/min)	512.65	682.41	285.52	326.31	674.17
v_1	(%)	13.91	14.62	6.25	8.04	15.53
v_2	(%)	0.01	0.01	0.00	0.35	0.00
PS	(ml/100ml/min)	0.29	0.26	0.00	3.31	0.09

IV. CONCLUSION

This paper has illustrated the feasibility of applying tracer kinetic modeling with DCE-MRI in a pre-clinical setting. We have shown the feasibility of applying a high temporal resolution (2 sec) protocol for arterial concentration estimation and liver imaging in mice. We observed a low value of interstitial space volume fraction and permeability-surface area product in normal mouse liver cases, which corresponded with murine liver physiology and the results previously obtained in the human studies. It indicates potentials of applying this technique for pre-clinical drug developments, as knowledge of these microcirculatory parameters may allow enhanced understanding of mechanism of drug action.

REFERENCES

[1] C.-I. Wong, T.-S. Koh, R. Soo, S. Hartono, C.-H. Thng, E. McKeegan, *et al.*, "Phase I and Biomarker Study of ABT-869, a Multiple Receptor Tyrosine Kinase Inhibitor, in Patients With Refractory Solid Malignancies," *Journal of Clinical Oncology,* vol. 27, pp. 4718-4726, 2009.

[2] C. Thng, T. Koh, D. Collins, and D. Koh, "Perfusion magnetic resonance imaging of the liver," *World Journal of Gastroenterology,* vol. 16, pp. 1598-1609, 2010.

[3] G. Liu, H. S. Rugo, G. Wilding, T. M. McShane, J. L. Evelhoch, C. Ng, *et al.*, "Dynamic Contrast-Enhanced Magnetic Resonance Imaging As a Pharmacodynamic Measure of Response After Acute Dosing of AG-013736, an Oral Angiogenesis Inhibitor, in Patients With Advanced Solid Tumors: Results From a Phase I Study," *J Clin Oncol,* vol. 23, pp. 5464-5473, 2005.

[4] B. Morgan, M. A. Horsfield, J. Stattaus, A. Khalil, T. C. Gauler, V. Gounant, *et al.*, "Dynamic contrast-enhanced magnetic resonance imaging (DCE-MRI) as a biomarker for the effect of PTK787/ZK 222584 (PTK/ZK) as second-line mono-therapy in patients with stage IIIB or stage IV non-small cell lung cancer (NSCLC)," *ASCO Ann. Meeting Proc,* vol. 25, p. 7676, 2007.

[5] B. Morgan, A. L. Thomas, J. Drevs, J. Hennig, M. Buchert, A. Jivan, *et al.*, "Dynamic Contrast-Enhanced Magnetic Resonance Imaging As a Biomarker for the Pharmacological Response of PTK787/ZK 222584, an Inhibitor of the Vascular Endothelial Growth Factor Receptor Tyrosine Kinases, in Patients With Advanced Colorectal Cancer and Liver Metastases: Results From Two Phase I Studies," *J Clin Oncol,* vol. 21, pp. 3955-3964, 2003.

[6] P. Antkowiak, R. Janiczek, L. Gibberman, C. Xu, C. Kramer, C. Meyer, *et al.*, "Quantitative first-pass perfusion MRI of the mouse heart," *Journal of Cardiovascular Magnetic Resonance,* vol. 12, p. M10, 2010.

[7] L. Jensen, K. Berge, T. Bathen, H. Wergedahl, S. Schønberg, A. Bofin, *et al.*, "Effect of Dietary Tetradecylthioacetic Acid on Colon Cancer Growth Studied by Dynamic Contrast Enhanced MRI," *Cancer biology & therapy,* vol. 6, pp. 1810-1816, 2007.

[8] J. Sedlacik, R. Williams, M. Johnson, C. Calabrese, A. M. Davidoff, and Hillenbrand, "Design and setup of dynamic contrast enhanced experiments for longitudinal preclinical studies of tumor response to anti-angiogenic therapy," *Proceedings of International Society of Magnetic Resonance in Medicine,* vol. 17, p. 3595, 2009.

[9] M. Widerøe, Ø. Olsen, T. B. Pedersen, P. E. Goa, A. Kavelaars, C. Heijnen, *et al.*, "Manganese-enhanced magnetic resonance imaging of hypoxic-ischemic brain injury in the neonatal rat," *NeuroImage,* vol. 45, pp. 880-890, 2009.

[10] T. S. Koh, C. H. Thng, P. S. Lee, S. Hartono, H. Rumpel, B. C. Goh, and S. Bisdas, "Hepatic Metastases: In Vivo Assessment of Perfusion Parameters at Dynamic Contrast-enhanced MR Imaging with Dual-Input Two-Compartment Tracer Kinetics Model1," *Radiology,* vol. 249, pp. 307-320, 2008.

[11] P. Hayton, M. Brady, L. Tarassenko, and N. Moore, "Analysis of dynamic MR breast images using a model of contrast enhancement," *Medical Image Analysis,* vol. 1, pp. 207-224, 1997.

[12] T. McDonald, R. Clift, and M. Cottrell, "Large, chronic doses of erythropoietin cause thrombocytopenia in mice [see comments]," *Blood,* vol. 80, pp. 352-358, 1992.

[13] D. R. Trune, J. B. Kempton, and N. D. Gross, "Mineralocorticoid receptor mediates glucocorticoid treatment effects in the autoimmune mouse ear," *Hearing Research,* vol. 212, pp. 22-32, 2006.

[14] E. Wisse, "An electron microscopic study of the fenestrated endothelial lining of rat liver sinusoids," *Journal of Ultrastructure Research,* vol. 31, pp. 125-150, 1970.

[15] E. Wisse, "An ultrastructural characterization of the endothelial cell in the rat liver sinusoid under normal and various experimental conditions, as a contribution to the distinction between endothelial and Kupffer cells," *Journal of Ultrastructure Research,* vol. 38, pp. 528-562, 1972.

[16] B. Smedsrød, P. J. De Bleser, F. Braet, P. Lovisetti, K. Vanderkerken, E. Wisse, and A. Geerts, "Cell biology of liver endothelial and Kupffer cells," *Gut,* vol. 35, pp. 1509-1516, 1994.

[17] J. Baratta, A. Ngo, B. Lopez, N. Kasabwalla, K. Longmuir, and R. Robertson, "Cellular organization of normal mouse liver: a histological, quantitative immunocytochemical, and fine structural analysis," *Histochemistry and Cell Biology,* vol. 131, pp. 713-726, 2009.

[18] L. Chiandussi, F. Greco, G. Sardi, A. Vaccarino, C. Ferraris, and B. Curti, "Estimation of hepatic arterial and portal venous blood flow by direct catheterization of the vena porta through the umbilical cord in man. Preliminary results," *Acta hepatosplenologica,* vol. 15, pp. 166-171, 1968.

[19] B. Davies and T. Morris, "Physiological Parameters in Laboratory Animals and Humans," *Pharmaceutical Research,* vol. 10, pp. 1093-1095, 1993.

[20] P. V. Pandharipande, G. A. Krinsky, H. Rusinek, and V. S. Lee, "Perfusion Imaging of the Liver: Current Challenges and Future Goals1," *Radiology,* vol. 234, pp. 661-673, 2005.

[21] T. S. Koh, C. H. Thng, S. Hartono, J. W. Kwek, J. B. K. Khoo, K. Miyazaki, *et al.*, "Dynamic contrast-enhanced MRI of neuroendocrine hepatic metastases: A feasibility study using a dual-input two-compartment model," *Magnetic Resonance in Medicine,* vol. 65, pp. 250-260, 2011.